The Astrophysical Journal, 638:878–886, 2006 February 20

LARGE PROPER MOTIONS IN THE JET OF THE HIGH-MASS YSO CEPHEUS A HW2

S. Curiel,[1,2] P. T. P. Ho,[2] N. A. Patel,[2] J. M. Torrelles,[3] L. F. Rodríguez,[4] M. A. Trinidad,[5] J. Cantó,[1] L. Hernández,[1] J. F. Gómez,[6,7] G. Garay,[8] and G. Anglada[7]

Received 2005 June 17; accepted 2005 October 18

ABSTRACT

Using high angular resolution (∼0.″25–0.″05) Very Large Array (VLA) observations made at 3.6 cm, 1.3 cm, and 7 mm during the period 1991–2004, we report the detection of large proper motions in the components of the radio continuum jet associated with the high-mass young stellar object (YSO) HW2 in the star-forming region Cepheus A. The relative proper motions observed for the two main components of the outflow, moving away from the central source in nearly opposite directions, are of the order of 140 mas yr^{-1}, or ∼480 km s^{-1} at a distance of 725 pc. The proper motions observed in the northeast and southwest lobes are not completely antiparallel, and the central elongated source seems to be changing orientation. We discuss possible scenarios to account for these and other observed characteristics. We also report the detection of a 7 mm compact continuum condensation of emission near the center of the thermal radio continuum jet, which we propose as the location of the exciting star.

Subject headings: ISM: individual (Cepheus A) — ISM: jets and outflows — radio continuum: ISM — stars: formation

1. INTRODUCTION

Cepheus A is a very active star formation region, located at a distance of about 725 pc (Johnson 1957; Sargent 1977) and containing the second source in the sky ever noted to exhibit the phenomenon of bipolar molecular outflow (Rodríguez et al. 1980). Subsequent observations showed that the CO outflow in this region is quite complex, having a quadrupolar or multipolar morphology and probably being powered by several YSOs (e.g., Bally & Lane 1990; Narayanan & Walker 1996). Several of the multiple radio continuum sources detected in this region seem to have internal sources, while others appear to be shock-excited and to delineate the edges of high-density molecular cores seen in NH_3 (e.g., Garay et al. 1996; Torrelles et al. 1993, 1998; Curiel et al. 2002; Martín-Pintado et al. 2005). The main driver of this complex outflow seems to be a thermal radio jet (probably a B0.5 zero-age main sequence star; Hughes et al. 1995; Rodríguez et al. 1994), known as HW2, which is the brightest of the radio continuum sources detected in the region (HW objects; Hughes & Wouterloot 1984), and is elongated at centimeter wavelengths in the northeast-southwest direction (position angle [P.A.] ∼ 45°). A bipolar HCO^+ outflow is centered at the position of HW2 and is well aligned with the thermal radio jet (Gómez et al. 1999). The bolometric luminosity of this high-mass star-forming region is $\simeq 2.5 \times 10^4\ L_\odot$ (Evans et al. 1981). Some of the radio continuum sources are associated with clusters of H_2O, OH, and CH_3OH masers (e.g., Lada et al. 1981; Cohen et al. 1984; Torrelles et al. 1996, 1998, 2001a, 2001b; Minier et al. 2000; Gallimore et al. 2003; Niezurawska et al. 2004; Bartkiewicz et al. 2005). In particular, the water masers associated with the HW2 radio jet are distributed in an elongated structure perpendicular to the jet, delineating possibly a circumstellar disk around this YSO (Torrelles et al. 1996), and magnetic fields between 100 and 500 mG have been measured in the central maser region (Vlemmings et al. 2006). In addition, recent subarcsecond Submillimeter Array (SMA) observations have revealed a flattened disklike structure in both dust and CH_3CN line emission of about 1000 AU in size and coinciding with, but perpendicular to, the HW2 radio continuum jet (Patel et al. 2005). Finally, millimeter observations, with an angular resolution of about 2″, have shown strong and unresolved dust emission associated with HW2, as well as weak compact emission associated with two other sources in this cluster of YSOs, suggesting that at least three of the continuum sources have circumstellar disks associated with them (Gibb et al. 2003; S. Curiel et al. 2006, in preparation).

In this paper we report new subarcsecond radio continuum observations of this region, carried out with the VLA. We have complemented these new data with archival VLA data (§ 2). We discuss the location of the high-mass protostar based on the 7 mm continuum observations (§ 3.1). We found that the radio continuum jet has two main components that are moving away in opposite directions from the central source (§ 3.2). In § 3.3 we discuss the physical properties of the radio continuum jet. We discuss the possibilities that the central source could be precessing and/or nutating, or that the central source itself could have proper motions (§ 3.4). Finally, we present some remarks on HW2 in § 4 and summarize our main conclusions in § 5.

2. OBSERVATIONS

The new observations were carried out with the VLA of the National Radio Astronomy Observatory (NRAO)[9] in the A

[1] Instituto de Astronomía, Universidad Nacional Autónoma de México (UNAM), Apartado Postal 70-264, 04510 México, DF, Mexico. On sabbatical leave at the Center for Astrophysics, Cambridge, MA; scuriel@astroscu.unam.mx, liliana@astroscu.unam.mx.

[2] Harvard-Smithsonian Center for Astrophysics, 60 Garden Street, Cambridge, MA 02138; scuriel@cfa.harvard.edu, pho@cfa.harvard.edu, npatel@cfa.harvard.edu.

[3] Instituto de Ciencias del Espacio (CSIC); and Institut d'Estudis Espacials de Catalunya, C/Gran Capità 2-4, E-08034 Barcelona, Spain. On sabbatical leave at United Kingdom Astronomy Technology Centre, Royal Observatory, Edinburgh, UK; torrelle@ieec.fcr.es.

[4] Centro de Radioastronomía y Astrofísica, UNAM, Apartado Postal 3-72 (Xangari), 58089 Morelia, Michoacán, Mexico; l.rodriguez@astrosmo.unam.mx.

[5] Departamento de Astronomía, Universidad de Guanajuato, Apartado Postal 144, 36240 Guanajuato, Guanajuato, Mexico; trinidad@astro.ugto.mx.

[6] Laboratorio de Astrofísica Espacial y Física Fundamental (INTA), Apartado Correos 50727, E-28080 Madrid, Spain.

[7] Instituto de Astrofísica de Andalucia (CSIC), Apartado 3004, E-18080 Granada, Spain; guillem@iaa.es, jfg@iaa.es.

[8] Departamento de Astronomía, Universidad de Chile, Casilla 36-D, Santiago, Chile; guido@das.uchile.cl.

[9] The National Radio Astronomy Observatory is a facility of the National Science Foundation operated under cooperative agreement by Associated Universities, Inc.

TABLE 1
Summary of the Observations

λ (cm)	Date	Phase Calibrator	Flux Density[a] (Jy)	Synthesized Beam FWHM (arcsec)	Synthesized Beam P.A. (deg)	rms (μJy beam^{-1})	Reference
1.3	2004 Oct 12	2200+420	3.60	0.09×0.07	9.9	260	1
3.6	2002 Feb 4	2322+509	2.41	0.27×0.19	−79.1	50	2
1.3	2002 Apr 23	2230+697	0.68	0.09×0.07	32.8	50	2
3.6	2000 Dec 23	2202+422	2.76	0.25×0.18	−28.8	40	3
3.6	1999 Jul 18	2322+509	1.6	0.34×0.21	−47.6	90	2
1.3	1999 Jul 18	2322+509	1.37	0.13×0.09	−27.3	770	2
0.7	1996 Dec 21	2229+695[b]	0.47	0.05×0.04	−57.9	250	3
1.3	1995 Jul 5	2200+420[b]	3.60	0.08×0.07	88.5	130	4
3.6	1991 Jul 7	2229+695[b]	0.57	0.25×0.19	33.1	40	3

[a] Bootstrapped flux densities in janskys.
[b] The 1996, 1995, and 1991 data were obtained using B1950.0 coordinates.
References.—(1) Patel et al. 2005; (2) this work; (3) Curiel et al. 2002; (4) Torrelles et al. 1996.

configuration at 3.6 and 1.3 cm during several epochs between 1999 and 2002 (see Table 1). These observations have an angular resolution of $\sim$0.″25 and 0.″08, at these two wavelengths, and resolve the Cepheus A HW2 radio continuum jet into two main outer elongated components and a central source. The observations were made in both circular polarizations, with an effective bandwidth of 100 MHz. The data were edited, calibrated, and imaged using the Astronomical Image Processing System (AIPS) software of the NRAO. We made cleaned images of the field, setting the ROBUST parameter of the AIPS task IMAGR to 0, to optimize the compromise between angular resolution and sensitivity. The synthesized beam dimensions and rms sensitivity of the multiepoch images, as well as the bootstrapped flux density of the respective phase calibrator, are listed in Table 1. We have not used the 1.3 cm map taken in 1999 July 18 in the present discussion because it is very noisy and the two main peaks of the central source are only marginally detected.

We have also compared these results with previous observations, using the 3.6 cm and 7 mm continuum data (Curiel et al. 2002) taken in 1991 July 7, 1996 December 21, and 2000 December 23, as well as the 1.3 cm data (Torrelles et al. 1996; N. Patel et al. 2006, in preparation) taken in 1995 July 5 and 2004 October 12. Contour maps of the continuum emission at 3.6 cm, 1.3 cm, and 7 mm are shown in Figure 1. All the data used in this paper were taken with the A configuration of the VLA, except for the 3.6 cm map taken in 2002, which was obtained with the VLA in the A configuration and the Pie Town link. The (u, v) data taken in coordinates B1950.0 were precessed to coordinates J2000.0 using the task UVFIX.

3. RESULTS AND DISCUSSION

The 3.6 cm maps (Fig. 1) resolve the Cepheus A HW2 radio continuum jet into a central source and two main outer components (labeled NE and SW). They are well aligned in the northeast-southwest direction with a P.A. of $\simeq$45°, delineating the orientation of the larger scale HCO^+ outflow. The outer condensations appear to be moving away from the central source in successive epochs (see § 3.2). The northeast and southwest condensations appear to be expanding as they move away from the central source, and their integrated flux densities (about 3.3 and 2.0 mJy in epoch 2002) have remained nearly constant with time (S. Curiel et al. 2006, in preparation). There is another peak located $\simeq$0.″5 to the south of the central source that nearly coincides with the center of the expanding spherical bubble of water masers detected with the Very Long Baseline Array (VLBA; Torrelles et al. 2001a; Curiel et al. 2002). This source will be discussed elsewhere (S. Curiel et al. 2006, in preparation). We also show in this figure the 1.3 cm and 7 mm images of HW2. The 1.3 cm and 7 mm data trace the inner part of the thermal radio continuum jet. At these wavelengths, the central source appears more compact than at 3.6 cm, elongated in the northeast-southwest direction with two main peaks and some extended emission either to the southwest or the northeast. The two extended, outer components of the radio continuum jet observed at 3.6 cm are not observed at these wavelengths, probably because they are resolved out by the higher angular resolution of the 1.3 cm and 7 mm ($\sim$0.″08 and 0.″05, respectively) observations and the lower sensitivity achieved at these wavelengths. The 1.3 cm images taken in 1995 and 2004 show an extra peak to the southwest from the two main peaks, nearly aligned with the outflow axis and associated with material ejected at different epochs (see discussion below). The 3.6 cm image taken in 1991 shows an extra peak to the northeast also aligned with the outflow axis, but associated with an earlier ejection of material (see discussion below). The 7 mm image, obtained with much higher angular resolution than the maps at other wavelengths, appears more complex, with four main peaks of emission in the northeast-southwest direction, all aligned with the radio continuum jet (see §§ 3.1 and 3.2). At this wavelength there is another faint peak to the south ($\sim$0.″15) that nearly coincides with a second group of water masers observed with the VLBA (Torrelles et al. 2001b; Curiel et al. 2002).

3.1. *Location of the Powering Source*

In contrast to the 3.6 cm maps that clearly show the outer components moving away from the central source (see Fig. 1 and discussion below), the two main components in the 1.3 cm maps stay basically in the same position, with some small oscillations around their mean position (see Table 2). This striking result implies that these components are not ejections from the powering source. We speculate that they could be associated with the outer part of the cavity evacuated in the infalling gas by the wind, and being shocked by the wind. On the other hand, the third peak toward the southwest observed in 1995 does not appear in the latter observations, which suggests that it was part of the outflow as discussed below. The 7 mm image, which was obtained with a higher angular resolution, seems different from the 1.3 cm images. It has four components along the outflow axis instead of the two or three peaks observed at 1.3 cm. When the 1995 1.3 cm

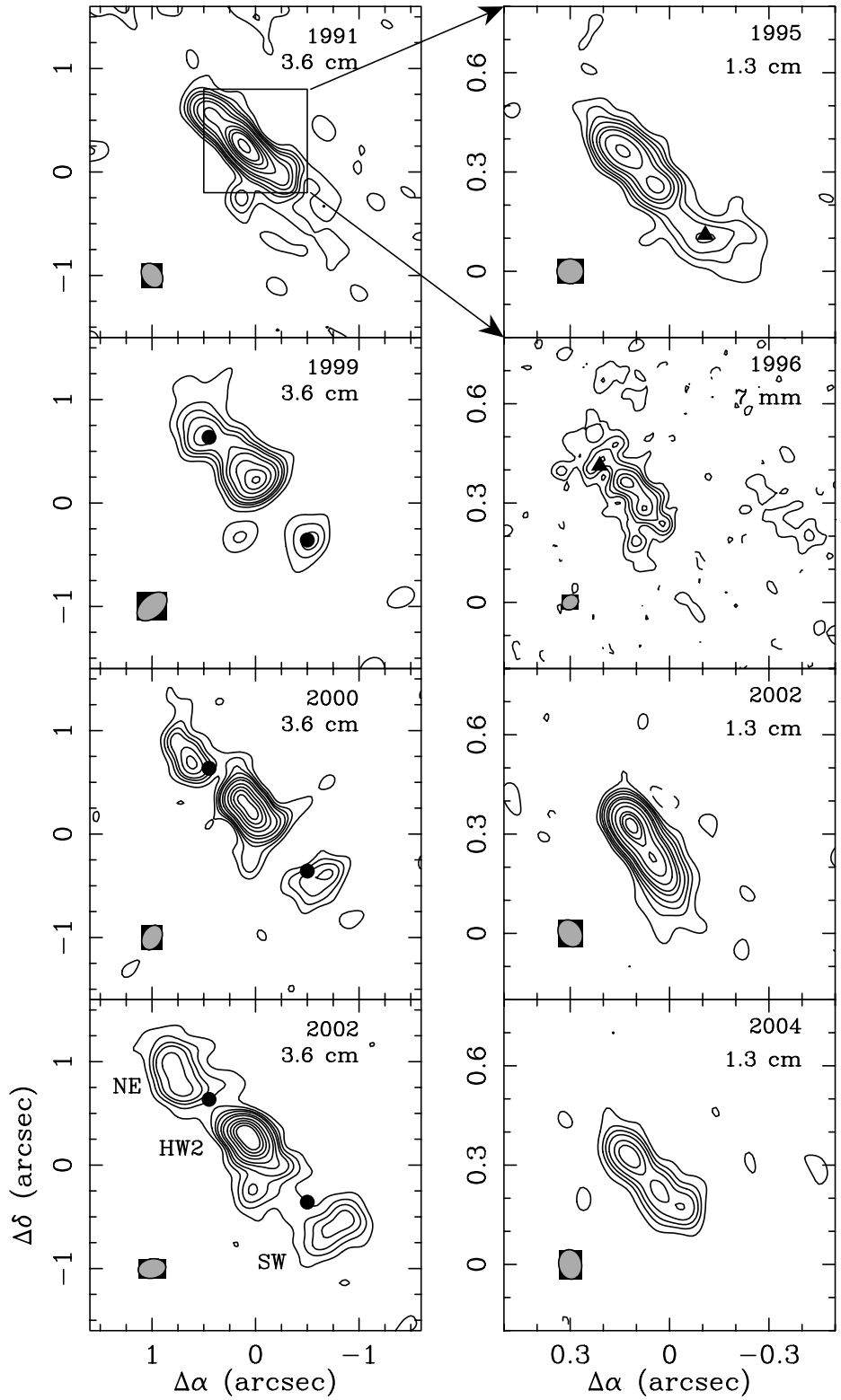

FIG. 1.—*Left*: Radio continuum VLA maps of the high-mass YSO HW2 at 3.6 cm. Contours are −4, −2, 2, 4, 6, 8, 12,16, 24, 32, 40, 48, 64, 80, and 96 × 40, 90, 40, and 50 μJy beam^{-1}, the rms noise of the maps taken in 1991, 1999, 2000, and 2002, respectively. The circles indicate the positions of the northeast and southwest knots for the 1999 epoch. The proper motions of these condensations are evident in subsequent epochs. The half-power contour of the beam is shown in each bottom left-hand corner. *Right*: Radio continuum VLA maps of the high-mass HW2 YSO at 1.3 cm and 7 mm. Contours are −6, −3, 3, 6, 9, 13, 20, 26, 38, 56, 75, 90, 105, and 120 × 130, 250, 50, and 260 μJy beam^{-1}, the rms noise of the maps taken in 1995, 1996, 2002, and 2004, respectively. The triangles indicate the positions where the southwest and northeast knots were observed for the first time (see 1995 and 1996 epochs). The half-power contour of the beam is shown in each bottom left-hand corner. In all the maps the (0, 0) coordinates correspond to the reference coordinates α(J2000.0) = $22^{\rm h}56^{\rm m}17\overset{\rm s}{.}971$, δ(J2000.0) = $62^{\circ}01'49\overset{''}{.}28$.

TABLE 2
OBSERVED PARAMETERS OF THE CENTRAL SOURCE

λ (cm)	DATE	α(J2000.0)[a] (s)	δ(J2000.0)[a] (arcsec)	SOURCE SIZE FWHM/Angular Separation[b,c] (arcsec)	SOURCE SIZE P.A.[d] (deg)	PEAK FLUX DENSITY[e] (mJy beam^{-1})	FLUX DENSITY[f] (mJy)
3.6.....	1991 Jul 7	17.9861	49.533	$0.726 \pm 0.007 \times 0.116 \pm 0.004$	46.5 ± 0.2	2.33 ± 0.003	8.5 ± 0.1
3.6.....	1999 Jul 18	17.9774	49.554	$0.383 \pm 0.008 \times 0.07 \pm 0.03$	45 ± 2	3.36 ± 0.08	7.1 ± 0.2
3.6.....	2000 Dec 23	17.9800	49.529	$0.442 \pm 0.005 \times 0.07 \pm 0.01$	41.4 ± 0.1	2.23 ± 0.03	6.0 ± 0.1
3.6.....	2002 Feb 4	17.9798	49.535	$0.360 \pm 0.003 \times 0.089 \pm 0.006$	36.2 ± 0.5	3.10 ± 0.02	6.85 ± 0.07
1.3.....	1995 Jul 7	17.9910	49.642	0.127 ± 0.004	43 ± 2	7.8 ± 0.1	37.9 ± 0.4
0.7.....	1996 Dec 21	17.9879	49.635	0.147 ± 0.004	40 ± 2	7.1 ± 0.3	65.0 ± 0.5
1.3.....	2002 Apr 23	17.9868	49.596	0.077 ± 0.004	34 ± 2	6.10 ± 0.04	18.5 ± 0.3
1.3.....	2004 Oct 12	17.9880	49.601	0.133 ± 0.004	41 ± 2	8.4 ± 0.3	33.7 ± 0.7

[a] Reference coordinates are $\alpha(\mathrm{J2000.0}) = 22^{\mathrm{h}}56^{\mathrm{m}}$, $\delta(\mathrm{J2000.0}) = 62^{\circ}01'$. Typical fitting errors are between 0.″002 and 0.″005. The coordinates at 1.3 cm and 7 mm are those of the northeast peak.
[b] Deconvolved size of the central source at 3.6 cm.
[c] Separation between the two main peaks observed at 1.3 cm and 7 mm (see § 3).
[d] Orientation of the central source at 3.6 cm and P.A. between the two peaks observed at 1.3 cm and 7 mm.
[e] Peak flux density of the central source at 3.6 cm and the northeast component at 1.3 cm and 7 mm, which is the strongest peak at all the observed epochs.
[f] Integrated flux density for the central source at 3.6 cm, 1.3 cm, and 7 mm.

and 1996 7 mm maps are overlapped (see Fig. 2), two peaks coincide spatially, while two other peaks (one at 1.3 cm and the other at 7 mm) lay outside this central structure and, as discussed below, are most likely associated with ejections from the central source.

There is a fourth peak of emission observed in the 7 mm map that does not coincide with any 1.3 cm peak and lies near the center of the radio continuum jet. In order to see if this component is embedded in the faint extended emission connecting the two main components seen at 1.3 cm, we made new 1.3 cm maps using superresolution by restoring the 1.3 cm maps with a beam of 0.″045, about 40% smaller than the original resolution and similar to that obtained at 7 mm. In these new maps there is a faint, compact component that coincides spatially with the 7 mm peak (see Fig. 3). We tentatively propose that this peak of emission indicates the location of the powering source. We have used the spatial coordinates of this peak, $\alpha(\mathrm{J2000.0}) = 22^{\mathrm{h}}56^{\mathrm{m}}17^{\mathrm{s}}.982$ and $\delta(\mathrm{J2000.0}) = 62^{\circ}01'49''.57$, with a positional uncertainty of about 0.″01, as the reference position for the proper-motion measurements that we present in § 3.2.

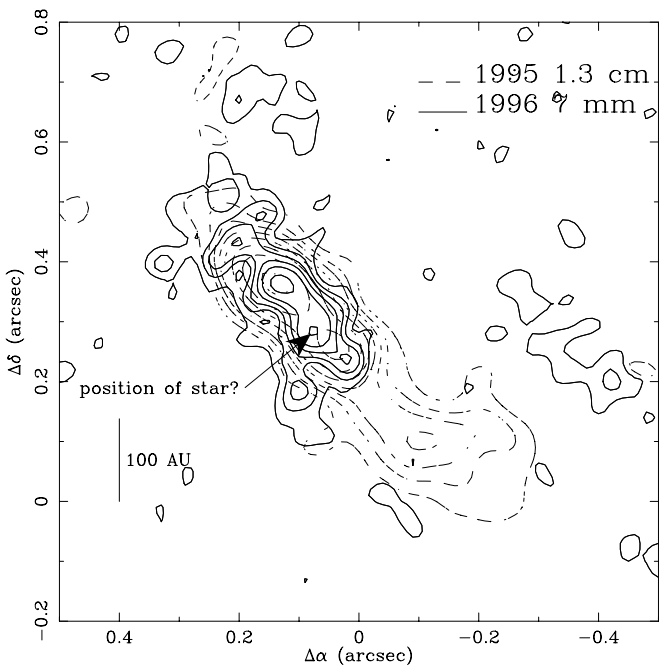

FIG. 2.—Overlay of the 1.3 cm (*dashed lines*) and 7 mm (*solid lines*) continuum maps of the YSO CepA/HW2 taken in 1995 and 1996. Contours are 3, 6, 9, 13, 18, 26, 38, and 56×130 and 250 μJy beam^{-1}, the rms noise of the maps. Two of the observed peaks at 1.3 cm and 7 mm coincide spatially. There is one peak to the northeast and another peak to the southwest observed at 7 mm and 1.3 cm, respectively, that seem to be gas ejected by the powering source. The extra peak observed at 7 mm, near the center of the main structure, may be associated with the powering star (see discussion). The beam sizes of the 1.3 cm and 7 mm maps are $0.''08 \times 0.''07$ with P.A. = 88.°5 and $0.''05 \times 0.''04$ with P.A. = −57.°9, respectively.

3.2. *Proper Motions*

Relative proper motions of the two outer components are evident in Figure 1. To study in detail these proper motions, we made a linear least-squares fit to the measured relative positions of both components (with respect to the position of the central star; see § 3.1) as a function of time, and the results are presented in Figures 4 and 5, and in Table 3. The positions of the observed components were obtained from Gaussian fits to the images made with the task IMFIT of AIPS and then by subtracting the position of the central star obtained at 7 mm for epoch 1996 (see § 3.1). For the northeast component we have used the positions obtained for the epochs 1999, 2000, and 2002 (at 3.6 cm), as well as for epoch 1996 (at 7 mm). In the case of the southwest component, we have used epochs 1999, 2000, and 2002 (at 3.6 cm), as well as epoch 1995 (at 1.3 cm). We have also included in these figures the measured positions of the other two components along the outflow, observed at two other epochs (in 1991 at 3.6 cm and in 2004 at 1.3 cm). The large span of time of these observations and large signal-to-noise ratio of the data, as well as the large proper motions of the condensations, allow us to estimate precise proper motions and orientations of these ejections. Furthermore, we find that the expected intrinsic errors of using different calibrators (typically of about 0.″05) do not change the present results significantly.

We find that the condensations are moving away from the central source in nearly straight lines (see Fig. 4) and with constant velocity (see Fig. 5). We do not find any evidence of acceleration or deceleration in a time span of about 11 yr. The proper motions for the northeast and southwest main components are 136 ± 3 and 143 ± 3 mas yr^{-1} (see Table 3), which imply at a distance of 725 pc a velocity in the plane of the sky of $\sim 470 \pm 10$ and

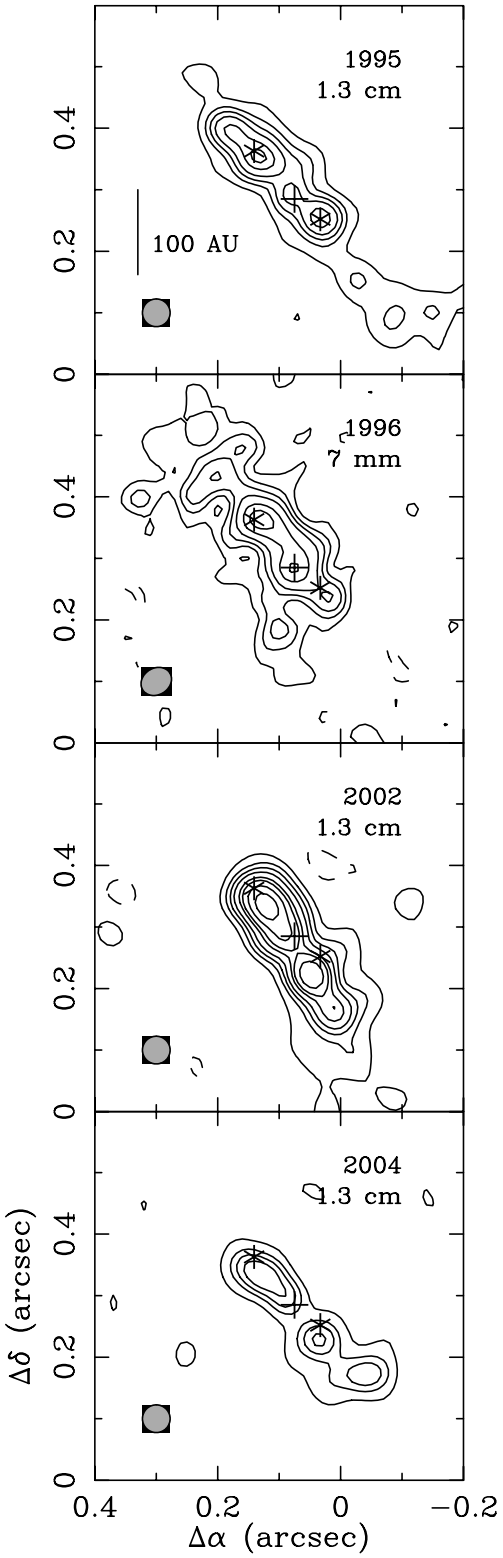

FIG. 3.—Radio continuum VLA maps of the high-mass HW2 YSO at 7 mm, as well as at 1.3 cm, obtained with a superangular resolution of 0.″045 (see discussion). Contours are −6, −3, 3, 6, 9, 13, 20, 26, 38, and 56 × 170, 250, 53, and 330 μJy beam^{-1}, the rms noise of the maps taken in 1995, 1996, 2002, and 2004, respectively. The asterisks mark the positions of the two main peaks observed at 1.3 cm in epoch 1995. The crosses indicate the position of the peak emission at 7 mm, located near the center of the radio jet, proposed to mark the location of the young star. The offset between the maps taken in 1995 and 1996 and those taken in 2002 and 2004 could be associated with either proper motions of HW2 or calibration errors (see discussion). The half-power contour of the beam is shown in each bottom left-hand corner.

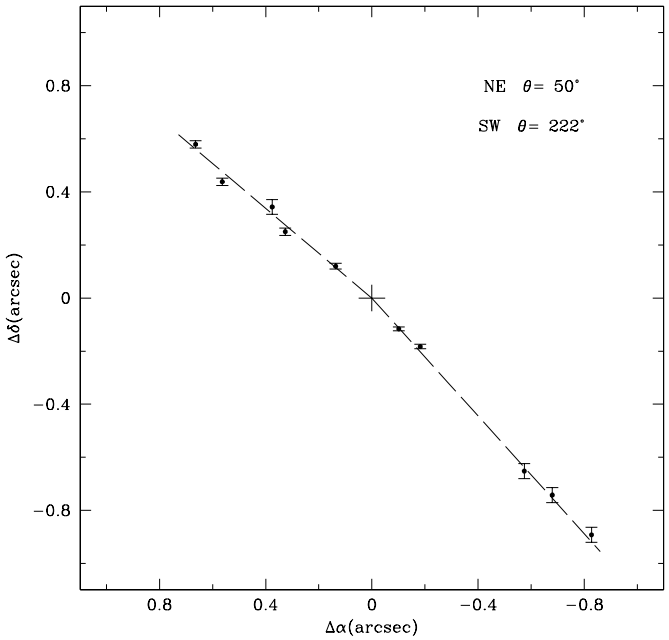

FIG. 4.—Relative proper motions of the northeast and southwest components along the radio continuum jet. The reference coordinates are α(J2000.0) = $22^h56^m17^s.9816$, δ(J2000.0) = 62°01′49″.572, the proposed location of the high-mass star (see discussion and Figs. 2 and 3). The dashed line corresponds to the fit of four observed positions along the outflow for each of the condensations. The error bars correspond to 2 σ measured values. The two points closest to the protostar position (the cross at the center) correspond to the peaks observed at 7 mm in the 1996 epoch (NE lobe) and the 1.3 cm in the 2004 epoch (SW lobe; see Fig. 1). The next two points outward correspond to the peaks observed at 3.6 cm in the 1991 epoch (NE lobe) and at 1.3 cm in the 1995 epoch (SW lobe). The three outermost points for both northeast and southwest lobes correspond to the peaks observed at 3.6 cm in the 1999, 2000, and 2002 epochs. The P.A.s of the measured proper motions are also shown. Note that the northeast and southwest components are moving away from the central source in slightly different directions.

490 ± 10 km s^{-1}, respectively. These tangential velocities are higher than those found at radio wavelengths in low-mass YSOs (∼100–300 km s^{-1}), such as the powering source of the HH1-2 system (Rodríguez et al. 2000) and the Serpens radio jet (Curiel et al. 1993, 1994; Raga et al. 2000). These proper motions are also much higher than those found in other outflows in this same high-mass star-forming region, which have velocities of the order of 100–300 km s^{-1} (Rodríguez et al. 2005; S. Curiel et al. 2006, in preparation). The proper motions that we report here are very similar to those found in the powering source of the HH 80/81 system (about 500 ± 120 km s^{-1}; Martí et al. 1998), which is also a high-mass YSO with a similar bolometric luminosity (∼2×10^4 $L_\odot$). We find that the spatial velocity of the outflow is between 525 and 650 km s^{-1} when we take into account the correction inferred from the inclination angle of the circumstellar disk (62° ± 10°) associated with this high-mass protostar (Patel et al. 2005).

In order to find the time at which the ejections occurred, we have assumed that the condensations were ejected from the same location within the central source. We find that the best fit to the data is obtained when using the position of the 7 mm condensation, which we propose marks the position of the powering star. Extrapolating back in time and assuming constant velocity (see Figs. 4 and 5), we estimate that the ejections of the northeast and southwest components took place in 1995.6 ± 0.2 and 1993.8 ± 0.2, respectively. Furthermore, there are other condensations along the radio continuum jet (see Fig. 1), observed at 3.6 cm in 1991 and at 1.3 cm in 2004, that seem to have been ejected at an earlier or later time, respectively (see Fig. 5). Assuming that this

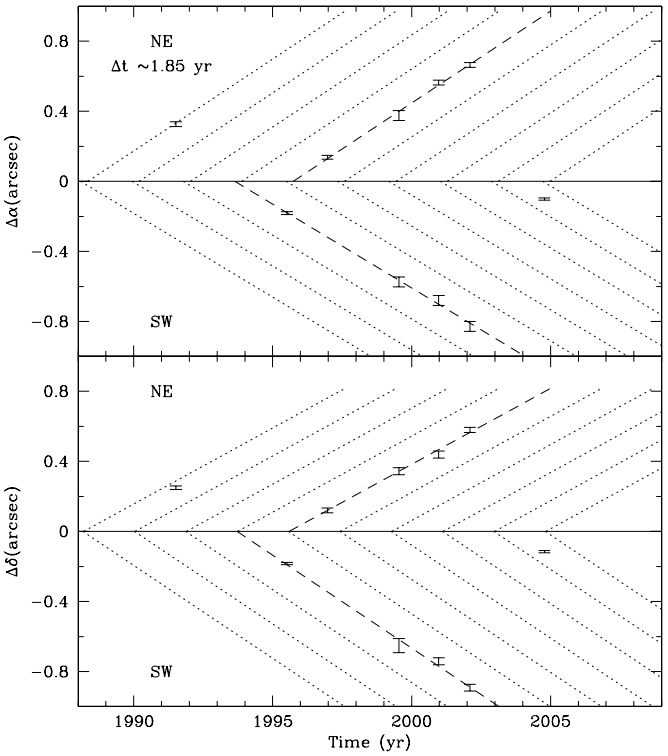

FIG. 5.—Right ascension and declination proper motions of the northeast and southwest components along the radio continuum jet. The error bars correspond to 2 σ measured values. The dashed lines correspond to the linear fits to the data. The parallel dotted lines indicate the expected positions of bipolar ejections from 1988 to 2005 every 1.85 yr. Note that an ejection frequency of about 1.85 yr not only explains the two main observed ejections (1995.6 and 1993.4), but also explains the ejections observed in 1991 (possibly ejected in 1988.2) and 2004 (possibly ejected in 2003.0).

high-mass YSO undergoes major ejections of material every 1.85 yr (the span of time between the two major ejections that we are reporting here), we find that the other two outflow components observed at 3.6 cm in 1991 and at 1.3 cm in 2004 were ejected around 1988.2 and 2003.0, respectively. Interestingly, by subtracting two 6 cm images taken in 1990 March 13 and 1991 July 6, Rodríguez et al. (2001) concluded that this YSO had a major bipolar ejection of gas in 1989.4 ± 0.2 and that the observed components were moving away from the central source with a tangential velocity of 950 ± 150 km s^{-1}. Their second 6 cm epoch and the 3.6 cm map in Figure 1 were obtained simultaneously, and thus the observed condensations are most likely the same. However, the condensation seen in the 3.6 cm map is not evident in the 6 cm map due to a coarser angular resolution. Their estimate for the time of the ejection 1989.4 ± 0.2 lies between two ejection epochs proposed here, 1988.2 and 1990.1 (see Fig. 5). In addition, the tangential velocity that they estimate for the 1989.4 ejection is about a factor of 2 larger than those found here for subsequent ejections in 1993.8 and 1995.6 ($\simeq$480 km s^{-1}). Such a difference in velocity, if significant, would suggest that the ejection velocity of the condensations may be varying with time. However, the fact that we find similar tangential velocities for the 1993.8 and 1995.6 ejections suggests that the velocity of the ejections does not change considerably with time. The difference between these two independent proper-motion measurements is probably due to the small span of time (and thus large errors) between the two 6 cm observations and the coarser angular resolution used by Rodríguez et al. (2001).

TABLE 3
PROPER MOTIONS

Component	μ_α (mas yr^{-1})	μ_δ (mas yr^{-1})	v (km s^{-1})	P.A. (deg)
Northeast.....	104 ± 2	88 ± 2	470 ± 10	50 ± 1
Southwest.....	-96 ± 2	-106 ± 2	490 ± 10	222 ± 1

3.3. *Physical Properties of the Radio Jet*

The physical properties of the radio jet can in principle be obtained from the flux density and the size of the radio continuum emitting regions, assuming that they are fully ionized, with a temperature of 10^4 K, and that the radio continuum emission is optically thin. Under these assumptions we estimate an electron density of about $(3-5) \times 10^4$ cm^{-3}, a mass of $\sim 10^{-7}\ M_\odot$, and a recombination time of about 3 yr for the ionized lobes. On the other hand, assuming a freely expanding biconical wind, the electron density in the HW2 ionized wind can be estimated by

$$\left[\frac{n_e(\phi)}{10^4\ \mathrm{cm}^{-3}}\right] = 8.79\left(\frac{\dot{M}_j}{10^{-7}\ M_\odot\ \mathrm{yr}^{-1}}\right)\left(\frac{d}{\mathrm{kpc}}\right)^{-2}\left(\frac{\phi}{\mathrm{arcsec}}\right)^{-2} \times \left(\frac{\theta_{\mathrm{op}}}{\mathrm{deg}}\right)^{-2}\left(\frac{v_j}{1000\ \mathrm{km\ s}^{-1}}\right)^{-1}\left(\frac{\mu}{1.2}\right)^{-1}, \quad (1)$$

where $n_e(\phi)$ is the electron density in the jet at an angular distance ϕ from the source, $\dot{M}_j$ is the total mass-loss rate of the source, d is the distance to the source, θ_{op} is the opening angle of the radio jet, v_j is the velocity of the wind, and μ is the mean atomic weight per electron. Then, the expected electron density at the distance of the radio lobes ($\sim$0.″7 or 507.5 AU) is $\sim 1.0 \times 10^4$ cm^{-3}, for a biconical stellar wind with a velocity of 500 km s^{-1}, an opening angle of 20° (see § 3.4), and a total mass-loss rate of $\sim 6 \times 10^{-7}\ M_\odot$ yr^{-1} (including both sides of the outflow). This electron density is several times lower than that estimated for the radio lobes. This result suggests that the observed lobes are produced by velocity perturbations in the stellar wind, similar to those proposed to explain the knots along the HH jets associated with low-mass YSOs (Raga et al. 1990).

Given that the radio lobes did not change substantially between 1999 and 2004 (see Fig. 1) and that their estimated recombination time is of only $\sim$3 yr, additional excitation seems necessary to maintain the lobes ionized for larger spans of times. Such excitation can in principle be provided by internal shocks, produced by velocity perturbations in the stellar wind, which produce the observed density enhancement and can survive several years before they fade away. In addition, the ionizing photons provided by the star, and that escape through the cavity carved by the outflow itself, can keep the gas photoionized at relatively large distances from this high-mass star. In fact, we find that less than 2% of the ionizing photons produced by the star and that travel through the lobes are necessary to maintain photoionized the gas in the outer condensations. In addition, Figure 1 shows that there is some faint, extended emission connecting the central source and the outer lobes and that extends farther out, which could be associated with the photoionized wind. Then, it seems plausible that the outer condensations will stay photoionized by the star for several more years before the expanding gas recombines and becomes neutral.

Assuming that the radio lobes are sections of a biconical ionized outflow moving away from the central source with a velocity of 500 km s^{-1} (the observed tangential velocity of the lobes)

and using the estimated mass for the northeast and southwest lobes, we obtain that the mass-loss rate carried by these mass ejections is about 2 and $5 \times 10^{-8}\ M_\odot\ \mathrm{yr}^{-1}$, respectively. On the other hand, the mass-loss rate of this YSO, obtained by using the parameters of the central source (assuming a jetlike morphology) is about $6 \times 10^{-7}\ M_\odot\ \mathrm{yr}^{-1}$, which is about an order of magnitude higher than the estimated total mass-loss rate carried away by these ejections ($\sim 7 \times 10^{-8}\ M_\odot\ \mathrm{yr}^{-1}$). This result also suggests that the observed radio lobes are velocity perturbations traveling along the stellar wind, and that the observed lobes are only a small fraction of the conical outflow.

The momentum rate injected by the highly collimated jet into the surrounding medium is $\sim 3 \times 10^{-4}\ M_\odot\ \mathrm{yr}^{-1}\ \mathrm{km\ s}^{-1}$. This momentum rate is about an order of magnitude lower than the momentum rate derived from the CO [$\sim (0.4\text{–}4) \times 10^{-3}\ M_\odot\ \mathrm{yr}^{-1}\ \mathrm{km\ s}^{-1}$] and HCO^+ [$\sim (5\text{–}8) \times 10^{-3}\ M_\odot\ \mathrm{yr}^{-1}\ \mathrm{km\ s}^{-1}$] molecular outflows (Hayashi et al. 1988; Narayanan & Walker 1996; Gómez et al. 1999). Thus, it appears that the HW2 radio jet does not have enough power to drive by itself the complex molecular outflow in the region. This indicates that the complex molecular outflow could be the superposition of multiple collimated outflows driven by some of the YSOs in the region.

3.4. *The Origin of the Asymmetry in the Radio Jet*

The northeast and southwest components are moving away from HW2 in nearly opposite directions and with similar proper motions. However, the P.A. of the northeast and southwest lobes (P.A. $= 50^\circ \pm 1^\circ$ and $222^\circ \pm 1^\circ$; see Table 3) are not exactly antiparallel. In this section we discuss two possible scenarios that can in principle explain the asymmetry observed in the two radio lobes. First, we argue that the asymmetry of the lobes could be due to proper motions of the star. Second, we argue that the observed velocity and orientation asymmetries in the lobes could be intrinsic to the source and due to temporal variations in both the wind velocity and the direction of the ejections.

3.4.1. *Proper Motions of the Star and Free-moving Ejections*

The measured difference of about 8° could be explained if the ejections of gas are bipolar, in opposite directions and moving freely through the ambient molecular gas (i.e., the resistance by the ambient gas is negligible), and they occur while the YSO is moving to the southeast. These assumptions seem adequate, since the condensations appear to be moving away from the star within the stellar wind. Thus, if we assume that the observed difference between the right ascension ([R.A.] and declination [decl.]) proper motions measured for the northeast and southwest components are due to the proper motions of the source, we find that this YSO would have proper motions of $\mu_\alpha = 4 \pm 4$ and $\mu_\delta = -9 \pm 4$ mas yr^{-1} (or a transverse velocity of 34 ± 20 km s^{-1} with P.A. $= 156^\circ \pm 24^\circ$). Subtracting the derived proper motions of the star, the proper motions of the northeast and southwest components would be $\simeq 139$ mas yr^{-1} (or 480 km s^{-1}) with P.A.s of $\simeq 46^\circ$ and 226°, respectively. The rough estimated transverse velocity of this YSO (about 34 ± 20 km s^{-1}) seems to be similar, given the estimated errors, to those found in YSOs in low-mass forming regions (about 15 km s^{-1}; e.g., Curiel et al. 2003; Rodríguez et al. 2003). Such a transverse velocity of HW2 could in principle be observed with high angular resolution observations taken several years apart. Figure 3 shows a small offset ($\leq 0\farcs05$) between the maps taken in 1995 and 1996 and those taken in 2002 and 2004 that could be associated with proper motions of HW2. However, this possible offset is smaller than that expected in a span of time of about 7 yr ($\sim 0\farcs07$), and it could also be due to the expected intrinsic errors of using different calibrators (typically of about $0\farcs05$). Further observations will be necessary to confirm if HW2 has proper motions with the inferred magnitude and orientation.

If we now assume that the outer condensations interact with the ambient molecular gas, as they move away from the central source, the observed bending of the jet could still be explained if the star moves to the southeast while ejecting material in opposite directions, similar to the freely moving case. However, in this case, the ejecta moving away from the source would be forced to slow down, due to its interaction with the gas in the dense core, while the YSO is moving toward the southeast. Thus, the main observational differences between this case and the freely moving case would be, first, that the velocity at which the condensations are ejected is larger than that measured with the present data, and second, that we should expect to see a deceleration in the lobes as they move through the high-density molecular core and away from the central star. However, as discussed in § 3.2, we do not find any evidence of acceleration or deceleration in a time span of about 11 yr. Thus, it seems more likely that the condensations move freely along the outflow and without interaction with the high-density ambient gas.

Finally, such large proper motions for HW2 would imply that the molecular cloud is also moving in a similar direction and with a similar velocity, or that this source has a large peculiar velocity. We estimate that the expected proper motions of a source at the location of Cepheus A due to the solar peculiar motions and the Galactic differential motions are about 2 mas yr^{-1} to the south, which is too small to explain the bending of the jet. In addition, the *Hipparcos* catalog shows that the visible stars in the OB association in the molecular cloud complex Cepheus OB3, to which Cepheus A belongs, within several degrees from HW2, have apparent proper motions between 2 and 6 mas yr^{-1} (or between 7 and 20 km s^{-1}) and with orientations mainly to the southwest (de Zeeuw et al. 1999), but with a large dispersion. These apparent proper motions are similar to those required for HW2 to explain the misalignment observed in the lobes of this radio jet. However, the orientation of the proper motions of the stars in the OB association is mainly to the southwest, while the required orientation is to the southeast. This makes it unlikely that the observed bending of the radio jet could be due to a possible peculiar velocity of the powering star.

3.4.2. *A Precessing and/or Nutating Powering Source?*

A second scenario to explain why the northeast and southwest radio continuum lobes are not completely antiparallel would be that the gas ejections of this YSO are bipolar but intrinsically in slightly different directions and with slightly different velocities. A closer look at the multiepoch maps shows that the orientation of the central source seems to change with time. The position, peak flux, and integrated flux density, as well as the Gaussian-fitted size and P.A., of the central source at 3.6 cm are listed in Table 2. For comparison, we also include in this table the measured separation and orientation between the two main peaks observed at 1.3 cm and 7 mm. The central source has a similar size at 3.6 cm in the different epochs, except for the 1991 epoch, where the measured size of the source may be affected by ejections emerging from the source (see Fig. 1). The separation between the two main peaks at 1.3 cm appears nearly constant at all the observed epochs. On the other hand, the P.A. of the central source at 3.6 cm seems to have decreased with time (about 10°) from 1991 to 2002. A similar trend is observed in the 1.3 cm maps, where the P.A. of the line joining the two main peaks also seems to have steadily decreased with time (about 10°) from 1995 to 2002, except for the last observed epoch (1.3 cm in 2004), when

the P.A. increased substantially from the previous observed epoch by about 8° (see Table 2).

At 3.6 cm, the central source appears elongated, having a deconvolved size of $\sim 0\farcs4 \times 0\farcs07$, with a mean P.A. of $\simeq 41^\circ$ (see Table 2). Thus, the source has an elongation ratio of about 6 (or even larger; see Table 2) and an opening angle (for a jetlike morphology) of about 20°. The measured size at 3.6 cm of $\simeq 0\farcs07$ for the minor axis of the central source suggests that collimation is present on scales of $\simeq$50 AU (for a distance of 725 pc). In addition, the measured P.A. of the major axis of the source (between 47° and 36°) is not aligned with the proper motions of the outer components (P.A. $= 50^\circ \pm 1^\circ$ and $222^\circ \pm 1^\circ$; see Table 2). All these characteristics are similar to those found in the driving sources of several low-mass YSOs, such as those of the HH 1–2 system (Rodríguez et al. 1990), the HH 111 system (Reipurth et al. 1999), and the Serpens radio jet (Curiel et al. 1993), where it has been argued that the misalignment between the orientation of the powering source and the outflow could be due to the source precessing and/or nutating because of a close companion. The individual maps show evidence of wiggling along the jet axis (see, for instance, the 1.3 cm maps in Fig. 1), which also suggests that the powering source could be precessing and/or nutating. In this case, there are two sources about 0.″15 and 0.″5 to the south of HW2 (see Figs. 1 and 3), but it is not clear if they could be gravitationally bound. In summary, we conclude that the remarkable characteristics of the HW2 radio jet (different orientations and velocities of the lobes, as well as the changing orientation of the central source) can be explained by a precessing and/or nutating powering source.

4. FINAL REMARKS

Finally, HW2 also has some characteristics that are very different from those found in low-mass YSOs. The tangential velocity measured in this radio jet ($\sim$500 km s^{-1}) is significantly larger than those found in low-mass YSOs ($\sim$100–300 km s^{-1}). The observed flux densities of HW2 (for instance, $\sim$7 mJy at 3.6 cm and $\sim$40 mJy at 1.3 cm) are much higher than those found in low-mass YSOs (up to a few millijanskys at both wavelengths), even without taking into account that the distance to Cepheus A (725 pc) is much greater than the typical distance to low-mass protostars (100–150 pc). The spectral index of HW2 at centimeter wavelengths is consistent with that expected from a photoionized stellar wind ($\alpha = 0.6$), while those measured in low-mass stars are consistent with either optically thin thermal free-free emission ($\alpha = -0.1$) or partially thick thermal free-free emission (typically $\sim$0.2). The water masers in this source are among the most luminous found in star-forming regions, and they are distributed in a flattened structure, probably delineating a circumstellar disk. In addition, the bolometric luminosity of this source ($2.5 \times 10^4\ L_\odot$; about half of which seems to be associated with this protostar) is much higher than those of low-mass YSOs (up to a few tens of $L_\odot$). All these characteristics are consistent with HW2 being a high-mass YSO. In particular, the double peak observed in this powering source at different wavelengths has not been observed so far in any low-, intermediate-, or high-mass YSOs.

5. CONCLUSIONS

We present results of high-sensitivity, multifrequency VLA radio continuum observations of the high-mass young stellar object HW2 in the Cepheus A high-mass star-forming region. These observations have shown that this radio source exhibits a bipolar, jetlike morphology with condensations of emission along both sides of the jet. These observations, taken during a time span of about 13 yr, have shown that the two main condensations along the radio continuum jet are moving away from the central source with about the same tangential velocity and in nearly opposite directions. The difference in direction and velocity of the northeast and southwest lobes, as well as the observed change in orientation of the central source, appear to be consistent with the powering source HW2 undergoing precessing and/or nutating motions. In addition, the present data indicate that the two condensations moving away from the central source were ejected at different times, which suggests that this YSO undergoes episodic and asymmetric ejection of material. In particular, the results indicate that HW2 underwent two major episodes of ejection separated by 1.85 yr. Finally, we propose that one of the condensations seen at the observed highest angular resolution marks the spatial location of this young high-mass star.

We thank an anonymous referee for very useful comments that helped to improve the presentation of the paper. S. C. acknowledges support from DEGAPA/UNAM and from CONACyT grants 33933-E and 43120-E. Author J. C. acknowledges support from CONACyT grants 41320-F and 43103-F. Authors G. A., J. F. G., and J. M. T. acknowledge support from MEC (Spain) grant AYA 2005-08523. G. A. acknowledges partial support from Junta de Andalucía (Spain). M. A. T. acknowledges support from PROMEP grant 103.5/04/2758 and CONACyT grant 33933-E.

REFERENCES

Bally, J., & Lane, A. P. 1990, in ASP Conf. Ser. 14, Astrophysics with Infrared Arrays, ed. R. Elston (San Francisco: ASP), 273
Bartkiewicz, A., Szymczak, M., Cohen, R. J., & Richards, A. M. S. 2005, MNRAS, 361, 623
Cohen, R. J., Rowland, P. R., & Blair, M. M. 1984, MNRAS, 210, 425
Curiel, S., Girart, J. M., Rodríguez, L. F., & Cantó, J. 2003, ApJ, 582, L109
Curiel, S., Moran, J., Rodríguez, L. F., & Cantó, J. 1994, Ap&SS, 216, 137
Curiel, S., Rodríguez, L. F., Moran, J., & Cantó, J. 1993, ApJ, 415, 191
Curiel, S., et al. 2002, ApJ, 564, L35
de Zeeuw, P. T., Hoogerwerf, R., de Bruijne, J. H. J., Brown, A. G. A., & Blaauw, A. 1999, AJ, 117, 354
Evans, N. J., II, et al. 1981, ApJ, 244, 115
Gallimore, J. F., Cool, R. J., Thornley, M. D., & McMullin, J. 2003, ApJ, 586, 306
Garay, G., Ramírez, S., Rodríguez, L. F., Curiel, S., & Torrelles, J. M. 1996, ApJ, 459, 193
Gibb, A. G., Hoare, M. G., Mundy, L. G., & Wyrowski, F. 2003, in IAU Symp. 221, Star Formation at High Angular Resolution, ed. M. G. Burton, R. Jayawardhana, & T. L. Bourke (San Francisco: ASP), 425
Gómez, J. F., Sargent, A. I., Torrelles, J. M., Ho, P. T. P., Rodríguez, L. F., Cantó, J., & Garay, G. 1999, ApJ, 514, 287
Hayashi, S. S., Hasegawa, T., & Kaifu, N. 1988, ApJ, 332, 354
Hughes, V. A., Cohen, R. J., & Garrington, S. 1995, MNRAS, 272, 469
Hughes, V. A., & Wouterloot, J. G. A. 1984, ApJ, 276, 204
Johnson, H. L. 1957, ApJ, 126, 121
Lada, C. J., Blitz, L., Reid, M. J., & Moran, J. M. 1981, ApJ, 243, 769
Martí, J., Rodríguez, L. F., & Reipurth, B. 1998, ApJ, 502, 337
Martín-Pintado, J., Jiménez-Serra, I., Rodríguez-Franco, A., Martín, S., & Thum, C. 2005, ApJ, 628, L61
Minier, V., Booth, R. S., & Conway, J. 2000, A&A, 362, 1093
Narayanan, G., & Walker, C. K. 1996, ApJ, 466, 844
Niezurawska, A., Szymczak, M., Cohen, R. J., & Richards, A. M. S. 2004, MNRAS, 350, 1409
Patel, N., et al. 2005, Nature, 437, 109
Raga, A. C., Binette, L., Cantó, J., & Calvet, N. 1990, ApJ, 364, 601
Raga, A. C., Curiel, S., Rodríguez, L. F., & Cantó, J. 2000, A&A, 364, 763
Reipurth, B., Yu, K. C., Rodríguez, L. F., Heathcote, S., & Bally, J. 1999, A&A, 352, L83

Rodríguez, L. F., Curiel, S., Cantó, J., Loinard, L., Raga, A., & Torrelles, J. M. 2003, ApJ, 583, 330
Rodríguez, L. F., Curiel, S., Ho, P. T. P., Torrelles, J. M., & Canto, J. 1990, ApJ, 352, 645
Rodríguez, L. F., Delgado-Arellano, V. G., Gómez, Y., Reipurth, B., Torrelles, J. M., Noriega-Crespo, A., Raga, A. C., & Cantó, J. 2000, AJ, 119, 882
Rodríguez, L. F., Garay, G., Curiel, S., Ramírez, S., Torrelles, J. M., Gómez, Y., & Velázquez, A. 1994, ApJ, 430, L65
Rodríguez, L. F., Moran, J., & Ho, P. T. P. 1980, ApJ, 240, L149
Rodríguez, L. F., Torrelles, J. M., Anglada, G., & Martí, J. 2001, Rev. Mex. AA, 37, 95
Rodríguez, L. F., Torrelles, J. M., Raga, A., Cantó, J., Curiel, S., & Garay, G. 2005, Rev. Mex. AA, 41, 435
Sargent, A. I. 1977, ApJ, 218, 736
Torrelles, J. M., Gómez, J. F., Rodríguez, L. F., Curiel, S., Anglada, G., & Ho, P. T. P. 1998, ApJ, 505, 756
Torrelles, J. M., Gómez, J. F., Rodríguez, L. F., Curiel, S., Ho, P. T. P., & Garay, G. 1996, ApJ, 457, L107
Torrelles, J. M., Verdes-Montenegro, L., Ho, P. T. P., Rodríguez, L. F., & Cantó, J. 1993, ApJ, 410, 202
Torrelles, J. M., et al. 2001a, Nature, 411, 277
———. 2001b, ApJ, 560, 853
Vlemmings, W. H. T., Diamond, P. J., van Langevelde, H. J., & Torrelles, J. M. 2006, A&A, in press (astro-ph/0510452)